PROCEEDINGS OF SPIE

SPIEDigitalLibrary.org/conference-proceedings-of-spie

Three-dimensional multispectral hand-held optoacoustic imaging with microsecond-level delayed laser pulses

X. Luís Deán-Ben, Erwin Bay, Daniel Razansky

X. Luís Deán-Ben, Erwin Bay, Daniel Razansky, "Three-dimensional multispectral hand-held optoacoustic imaging with microsecond-level delayed laser pulses," Proc. SPIE 9323, Photons Plus Ultrasound: Imaging and Sensing 2015, 93231N (11 March 2015); doi: 10.1117/12.2080300



Event: SPIE BiOS, 2015, San Francisco, California, United States

Three-dimensional multispectral hand-held optoacoustic imaging with microsecond-level delayed laser pulses

X Luís Deán-Ben and Erwin Bay and Daniel Razansky *

Institute for Biological and Medical Imaging, Technical University of Munich and Helmholtz Center Munich, Ingolstädter Landstraße 1, 85764 Neuherberg, Germany.

ABSTRACT

Three-dimensional hand-held optoacoustic imaging comes with important advantages that prompt the clinical translation of this modality, with applications envisioned in cardiovascular and peripheral vascular disease, disorders of the lymphatic system, breast cancer, arthritis or inflammation. Of particular importance is the multispectral acquisition of data by exciting the tissue at several wavelengths, which enables functional imaging applications. However, multispectral imaging of entire three-dimensional regions is significantly challenged by motion artefacts in concurrent acquisitions at different wavelengths. A method based on acquisition of volumetric datasets having a microsecond-level delay between pulses at different wavelengths is described in this work. This method can avoid image artefacts imposed by a scanning velocity greater than 2 m/s, thus, does not only facilitate imaging influenced by respiratory, cardiac or other intrinsic fast movements in living tissues, but can achieve artifact-free imaging in the presence of more significant motion, e.g. abrupt displacements during handheld-mode operation in a clinical environment.

Keywords: Three-dimensional imaging, real-time imaging, hand-held probe, multispectral imaging.

1. INTRODUCTION

Optoacoustic (photoacoustic) imaging is increasingly being accepted in biological research since it allows for high-resolution imaging of optical absorption beyond the limits imposed by light diffusion, thus, otherwise undetactable or invisible anatomy and function can now be visualized at millimeter to centimeter scale depths in living organisms. Translation into clinical practice occurs to be the natural next step to fully exploit the exclusive capacities offered by this technology. Thereby, several dedicated systems using endoscopic, hand-held, or stationary design approaches have been recently proposed for clinical use, with multiple applications envisioned. Poparticular convenience is real-time imaging using hand-held probes, which permits visualization of dynamic events, speeds up clinical examinations and enables broad range of applications. These important advantages are also the main assets of ultrasonography, which is arguably the most widely applied imaging modality in today's clinical practice. On the other hand, the optoacoustic tomographic reconstruction problem and physics behind the signal excitation substantially differ from ultrasound imaging. Indeed, curved array geometry proved to be more efficient for collection of optoacoustic responses and further resulted in more accurate reconstructions. In 1,12 Furthermore, by acquisition of images at multiple optical wavelengths, multi-spectral optoacoustic tomography (MSOT) can map functional contrast as well as bio-distribution of molecular agents in tissues.

Real-time acquisition of multispectral datasets imposes significant technological challenges when considering motion in living subjects, e.g. due to breathing or heartbeat. Even more significant motion-associated problems can occur when operating optoacoustic imaging devices in a hand-held mode. Attempts to avoid motion-related artifacts in multispectral optoacoustic imaging were done using high repetition lasers.^{5,14} The single detector approach has only rendered two dimensional real-time performance for these implementations and was overall not suitable for hand-held operation. On the other hand, several systems allowing three-dimensional imaging in real time have been suggested.^{15–17} More importantly, a true five dimensional optoacoustic tomographic imaging framework has been showcased by fast laser wavelength tuning and real-time acquisition and visualization of three-dimensional multispectral data using spherical array detection geometry.¹³ Yet, the substantial (millisecond

*E-mail: dr@tum.de

Photons Plus Ultrasound: Imaging and Sensing 2015, edited by Alexander A. Oraevsky, Lihong V. Wang Proc. of SPIE Vol. 9323, 93231N ⋅ © 2015 SPIE ⋅ CCC code: 1605-7422/15/\$18 doi: 10.1117/12.2080300

level) time delay between laser pulses at different wavelengths limits the applicability of the approach in the handheld mode by introducing significant motion artifacts when the velocity of the probe exceeded several mm/s. The displacement d of the probe between two consecutive laser pulses is given by d = c/PRF, where c is the scanning velocity and PRF is the pulse repetition frequency of the laser. If more than two wavelengths are used for acquisition of the multispectral data, the motion constraint becomes proportionally more significant, further hampering real-time functional imaging in the presence of motion in the object or due to the handheld operation.

Herein, we discuss on the feasibility of functional volumetric (three-dimensional) optoacoustic imaging by introducing a microsecond-range delay between laser pulses at two different wavelengths. In this way, the delay between two images acquired at the different wavelengths is minimized, eliminating potential motion artifacts and enabling functional multispectral imaging even in the presence of abrupt displacements in the sample.

2. MATERIALS AND METHODS

2.1 Experimental set-up

For acquisition of multispectral data in real-time, two tunable OPO lasers (Phocus, Opotek Inc., Carlsbad, CA) were synchronized as described in 18. The lay-out of the experimental system employed is depicted in Fig. 1a. The OPO lasers were set at wavelengths 760 nm and 850 nm. The two beams were guided through a custommade fiber bundle (CeramOptec GmbH, Bonn, Germany) having two input arms and a common output arm. The optical fibers at the output of the bundle are randomly distributed with respect to the two inputs, i.e., both beams render approximately the same illumination profile at the tissue surface. The first laser was triggered internally. On the other hand, the flash lamps and Q-switch of the second laser were externally triggered and delayed with respect to the Q-switch output of the first laser (Fig. 1b). Two delay generators were used in the synchronization scheme. The first delay D1 was selected so that D1=T-L, where T and L represent respectively the pulse interval and the time lapse between the two laser pulses. The time lapse L needs to be sufficiently long to separate the optoacoustic time resolved signals corresponding to both laser pulses, which are recorded in the same time acquisition window. For T=100 ms (10Hz pulse repetition frequency), a value of 99.983 ms was chosen for D1, which corresponds to a time lapse of L=17 μ s between the Q-switch trigger signals of the two lasers. This time lapse represents approximately 27 mm of propagation of the ultrasound wave within tissue, which is larger than the imaged region of interest. The flash lamps of the second laser need also to be externally synchronized. To ensure optimal laser beam energy, a delay of C=180 μ s was established between the respective trigger signals. This was maintained by setting the delay of the second delay generator D2 to a value of 99.820 ms according to D2=T-C.

A spherical array optoacoustic hand-held probe was used to acquire three-dimensional tomographic data in real time. The consists of an array of 256 piezoelectric elements with a central frequency of 4 MHz and -6dB bandwidth of approximately 100%. The detection elements are densely distributed over a spherical surface with radius of 4 cm covering a solid angle of approximately 90°. The three-dimensional imaging probe supports nearly isotropic spatial resolution of 200 μ m in a volume of approximately 1 cm³ surrounding the center of the sphere. The output arm of the fiber bundle is inserted in a cylindrical cavity in the center of the hand-held probe to provide optical illumination along the central axis of the array. Acoustic coupling to the imaged part is ensured with a water-containing transparent polyethylene membrane. Acoustic gel was further applied for optimal acoustic coupling between the patient's skin and the membrane. The pressure signals at the 256 locations of the array elements are simultaneously collected with a sampling frequency of 40 megasamples per second at 2030 instants, immediately following the trigger signal of the first laser pulse. A custom-designed data acquisition system (Falkenstein Mikrosysteme GmbH, Taufkirchen, Germany) is used for simultaneous digital sampling of the analog data from the 256 channels. The acquisition is triggered with the Q-switch output of the first laser, and the acquired signals are subsequently transmitted to a personal computer through a 1 Gbit ethernet connection.

2.2 Hand-held scanning experiment

Optoacoustic signals were acquired for a hand-held scanning experiment in a human healthy volunteer. The imaging experiment was performed in full accordance with work safety regulations of Helmholtz Zentrum Munchen.

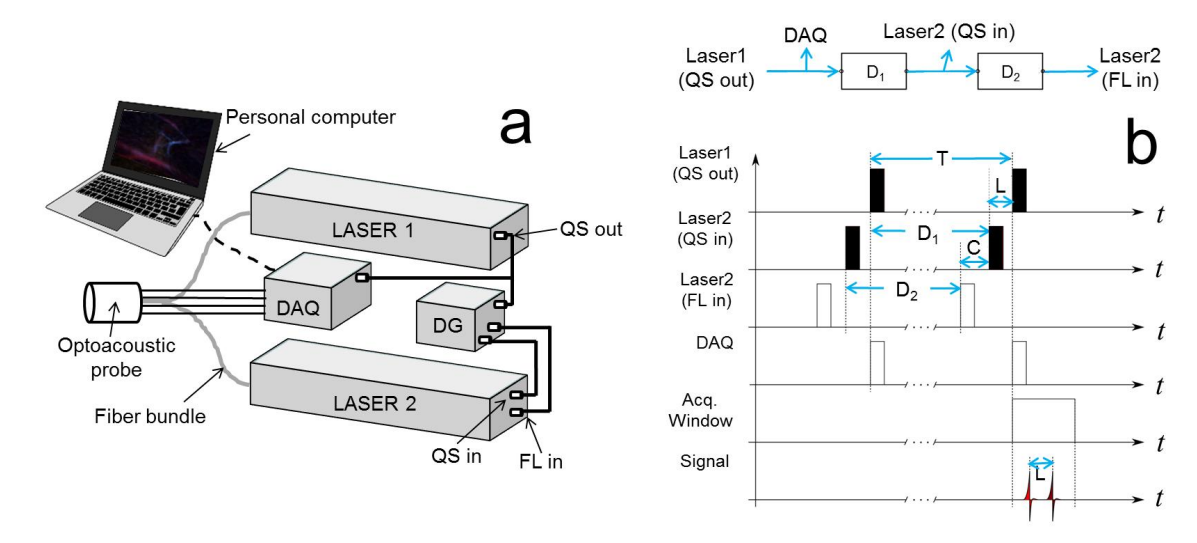


Figure 1. (a) Lay-out of the experimental system. DAQ - Data acquisition system. DG - delay generator. QS - Q-switch. FL - flash lamps. (b) Synchronization scheme between the two lasers.

The optoacoustic responses due to pulses at two different wavelengths can be separated on a time axis without cross talk. For image reconstruction, the acquired signals are first deconvolved with the electrical impulse response of the transducer and band-pass filtered between 0.2 and 7 MHz. A model-based reconstruction algorithm is then applied to reconstruct the absorbed energy map for each wavelength. Since measurements at only two wavelengths are available for the current proof-of-concept experiments, the absorption of light is further assumed to be only due to contributions of oxygenated (HbO2) and deoxygenated (Hb) hemoglobin. In order to isolate the contribution of the two chromophoric components, a spectral unmixing procedure based on a per-pixel least square fitting of the absorbed energy to a combination of oxygenated and deoxygenated hemoglobin was performed.

3. RESULTS

The palm of a healthy volunteer was scanned in a hand-held manner. The results of the imaging experiment are showcased in Fig. 2. The first and second columns display examples of maximum intensity projection (MIP) images acquired respectively at 760 nm and 850 nm. For the same imaged volume, images acquired at 850 nm show a different appearance than those corresponding to 760 nm, which is mostly related to the strong wavelength-dependent absorption by the blood chromophores. For instance, the highly oxygenated vessels (arteries) are naturally expected to present a higher optoacoustic intensity for the 850 nm wavelength as compared to 760 nm, whereas an opposite effect shall occur for less oxygenated vessels (veins). This is best perceived in the blood oxygen saturation maps displayed in the third column, where red and blue correspond to the distribution of oxygenated and deoxygenated hemoglobin respectively.

To compare the performance of method described herein to the fast wavelength tuning approach, we attempted to perform image unmixing by using instead the data from two adjacent laser pulses separated by approximately 100 ms. The reconstructed images (MIP along the depth direction) at 760 nm and 850 nm obtained with the synchronized laser pulses and with two adjacent pulses are displayed in the first and second rows of Fig. 2 respectively. The unmixed distributions of oxygenated and deoxygenated haemoglobin are displayed in the third column. Motion artefacts are clearly present for adjacent laser pulses. For example, the different oxygenation levels in the three vessels located in the central part of the image (labeled A) are only distinguished with the microsecond-delay approach. On the other hand, the vessels labeled B and C in the figure are shifted by approximately 800 μ m between adjacent pulses, which correspond to a scanning speed of 8 mm/s. Oxygenation errors can persist even if motion correction is performed. For example, vessel B appears to have a higher absorption at 760 nm than at 850 nm for images corresponding to adjacent pulses. This is due to a change in

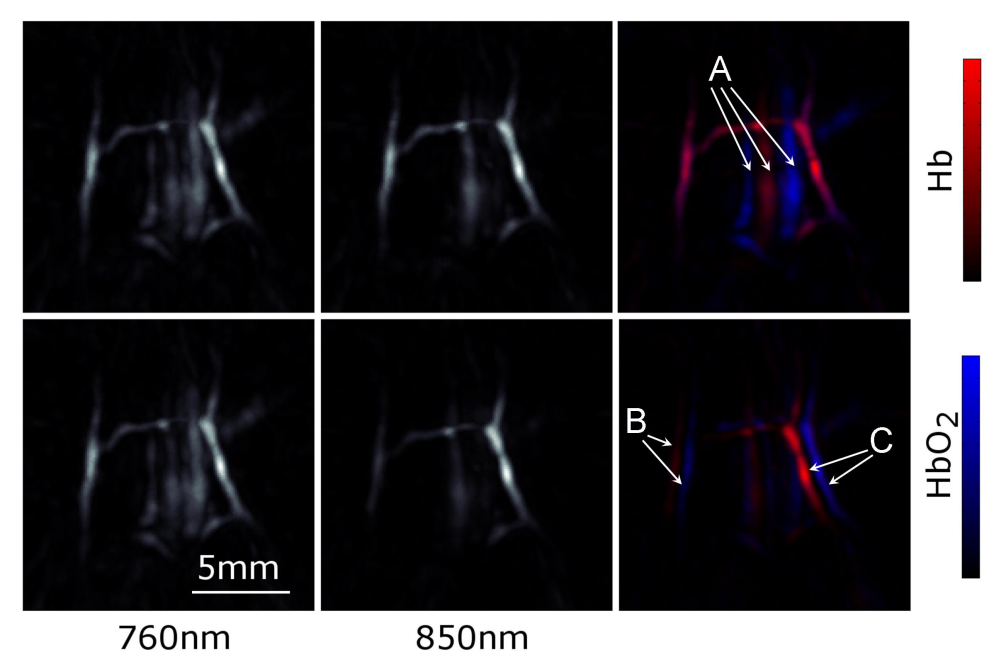


Figure 2. (a) Maximum intensity projection of the volumetric images at 760 nm. (b) Maximum intensity projection of the volumetric images at 850 nm. (c) Distribution of oxygenated (red) and deoxygenated hemoglobin (blue). The images in the first row corresponds to the two laser pulses delayed by 17 μ s and the images in the second row have a delay corresponding to subsequent laser pulses of the same laser.

the sensitivity of the transducer for different positions, but can be erroneously interpreted as a low oxygenation saturation in the vessel.

4. DISCUSSION AND CONCLUSIONS

The presented results showcase the feasibility of three-dimensional real-time functional imaging in the presence of relative motion between the object and the optoacoustic probe. Thus, motion-free multispectral images can be retrieved not only in the presence of intrinsic tissue motion, such as cardiac or breathing movements, but also when fast scanning with a hand-held probe is performed. For the dual wavelength approach described herein, even moving the probe at an unreasonably high velocity of 2 m/s would only result in a displacement of $34\,\mu\mathrm{m}$ within the 17 $\mu\mathrm{s}$ delay between laser pulses, which is below the spatial resolution of the three dimensional imaging probe. In this way, the multispectral hand-held scanning can be performed with low laser repetition rates of several pulses per second and high per-pulse energies in the tens and hundreds millijoule range, thus guaranteeing good signal-to-noise at deep locations. On the other hand, the repetition rate of the laser must be increased in order to reduce motion artifacts in conventional multispectral optoacoustic tomography using a single laser source. However, increasing the pulse repetition rate would readily imply corresponding reduction of the per-pulse energies in order to conform to the laser safety standards on the average light intensities delivered to the imaged subject, which would consequently compromise the signal-to-noise levels and the deep tissue imaging capacity.

The presented approach requires the use of two or more laser sources depending on the number of acquired wavelengths. This comes at the expense of a higher implementation cost and more design complexity of the data acquisition system and synchronization electronics. Thus, ideally, alternative methods shall be sought for generation of multiple pulses with microsecond delays. While generation of low energy pulses in the nanojoule and microjoule range with microsecond level delays is indeed possible using pulsed laser diodes, a different technology will be necessary to manufacture affordable devices for deep tissue multispectral imaging with pulse energies in the millijoule range.

In conclusion, it is anticipated that the presented functional three-dimensional optoacoustic imaging approach free of motion artifacts will further prompt introduction of the optoacoustic imaging technology into clinical practice.

ACKNOWLEDGMENTS

The research leading to these results received funding from the European Research Council under grant agreement ERC-2010-StG-260991.

REFERENCES

- [1] Wang, L. V. and Hu, S., "Photoacoustic tomography: in vivo imaging from organelles to organs," *Science* 335(6075), 1458–1462 (2012).
- [2] Ma, R., Distel, M., Deán-Ben, X. L., Ntziachristos, V., and Razansky, D., "Non-invasive whole-body imaging of adult zebrafish with optoacoustic tomography," *Physics in Medicine and Biology* **57**(22), 7227–7237 (2012).
- [3] Hudson, S. V., Huang, J. S., Yin, W., Albeituni, S., Rush, J., Khanal, A., Yan, J., Ceresa, B. P., Frieboes, H. B., and McNally, L. R., "Targeted noninvasive imaging of egfr-expressing orthotopic pancreatic cancer using multispectral optoacoustic tomography," *Cancer research* **74**(21), 6271–6279 (2014).
- [4] Jokerst, J. V., van de Sompel, D., Bohndiek, S. E., and Gambhir, S. S., "Cellulose nanoparticles are a biodegradable photoacoustic contrast agent for use in living mice," *Photoacoustics* **2**(3), 119–127 (2014).
- [5] Yang, J. M., Favazza, C., Chen, R., Yao, J., Cai, X., Maslov, K., Zhou, Q., Shung, K. K., and Wang, L. V., "Simultaneous functional photoacoustic and ultrasonic endoscopy of internal organs in vivo," *Nature Medicine* 18(8), 1297–1302 (2012).
- [6] Deán-Ben, X. L. and Razansky, D., "Functional optoacoustic human angiography with handheld video rate three dimensional scanner," *Photoacoustics* **1**(3), 68–73 (2013).
- [7] Fehm, T. F., Deán-Ben, X. L., and Razansky, D., "Four dimensional hybrid ultrasound and optoacoustic imaging via passive element optical excitation in a hand-held probe," Applied Physics Letters 105(17), 173505 (2014).
- [8] Heijblom, M., Piras, D., Xia, W., van Hespen, J. C. G., Klaase, J. M., van den Engh, F. M., van Leeuwen, T. G., Steenbergen, W., and Manohar, S., "Visualizing breast cancer using the twente photoacoustic mammoscope: What do we learn from twelve new patient measurements," Optics Express 20(11), 11582–11597 (2012).
- [9] Pang, G. A., Bay, E., Deán-Ben, X. L., and Razansky, D., "Three-dimensional optoacoustic monitoring of lesion formation in real time during radiofrequency catheter ablation," *Journal of Cardiovascular Electro*physiology (2014). doi:10.1111/jce.12584.
- [10] Beard, P., "Biomedical photoacoustic imaging," Interface Focus 1(4), 602–631 (2011).
- [11] Buehler, A., Kacprowicz, M., Taruttis, A., and Ntziachristos, V., "Real-time handheld multispectral optoa-coustic imaging," *Optics Letters* **38**(9), 1404–1406 (2013).
- [12] Deán-Ben, X. L., Ozbek, A., and Razansky, D., "Volumetric real-time tracking of peripheral human vasculature with gpu-accelerated three-dimensional optoacoustic tomography," *IEEE Transactions on Medical Imaging* 32(11), 2050–2055 (2013).
- [13] Deán-Ben, X. L. and Razansky, D., "Adding fifth dimension to optoacoustic imaging: volumetric time-resolved spectrally enriched tomography," *Light: Science & Applications* **3**(1), e137 (2014).
- [14] Wang, L., Maslov, K., and Wang, L. V., "Single-cell label-free photoacoustic flowoxigraphy in vivo," *Proceedings of the national academy of sciences of the USA* **110**(15), 5759–5764 (2013).
- [15] Buehler, A., Deán-Ben, X. L., Claussen, J., Ntziachristos, V., and Razansky, D., "Three-dimensional optoacoustic tomography at video rate," Optics Express 20(20), 22712–22719 (2012).
- [16] Xiang, L., Wang, B., Ji, L., and Jiang, H., "4d photoacoustic tomography," Scientific Reports 3, 1113 (2013).
- [17] Deán-Ben, X. L. and Razansky, D., "Portable spherical array probe for volumetric real-time optoacoustic imaging at centimeter-scale depths," Optics Express 21(23), 28062–28071 (2013).

- [18] Deán-Ben, X. L., Bay, E., and Razansky, D., "Functional optoacoustic imaging of moving objects using microsecond-delay acquisition of multispectral three-dimensional tomographic data," *Scientific Reports* 4, 5878 (2014).
- [19] Deán-Ben, X. L., Buehler, A., Ntziachristos, V., and Razansky, D., "Accurate model-based reconstruction algorithm for three-dimensional optoacoustic tomography," *IEEE Transactions on Medical Imaging* **31**(10), 1922–1928 (2012).